# Electron Temperature Determination from Non-LTE Populations in a Nitrogen Plasma JET

A. Catherinot and A. Sy

Laboratoire de Physique des Milieux Ionisés Université d'Orléans
Orleans Cedex (France)

(Z. Naturforsch. **30 a**, 1143–1155 [1975]; received May 28, 19975)

Atomic nitrogen electronic state populations and electron density have been measured in a high power nitrogen plasma jet in the pressure range $50 < P$ (Torr) $< 150$. A Boltzmann plot of the excited state populations led to electronic excitation temperatures depending on the groups of levels considered. Low and high lying levels yielded excitation temperatures which differed up to 80% at $P = 120$ Torr. The measured data are analysed in the frame of a two-temperatures diffusion-dominated plasma model.

## I. Introduction

Non-equilibrium behavior of plasmas has been widely studied in recent years both theoretically and experimentally [1–14]. The observed and calculated departures from equilibrium are ascribed to thermochemical non-equilibrium (electrons and heavy particles are at different temperatures and electron density does not satisfy the Saha equation) and excitational non-equilibrium (bound states of atoms are not populated according to the Boltzmann distribution). Among the properties that characterize such plasmas, the most important ones are electron density and electron temperature because these two parameters determine mainly the transport and radiative properties of a plasma. The electron density can be determined with a good precision, at relatively high electrons densities ($n_e > 10^{14}$ cm$^{-3}$), from Stark broadening of spectral lines. On the other hand, the electron temperature determination by conventional spectroscopic methods demands, at least, a partial LTE distribution amongst the levels involved and the free electrons. Especially, it has been shown theoretically [5, 11] that strong diffusion may, under certain conditions, destroy any possibility of determining the electron temperature from a Boltzmann plot.

During the past years, the most detailed experimental studies of this problem have been performed for argon, helium and hydrogen plasmas with special attention to wall-stabilized arcs at atmospheric pressure. Here we study an electric and magnetic fields free nitrogen plasma jet in the pressure range $50 < P$(Torr) $< 150$. The results show that the Boltzmann slope is indeed not further a characteristic quantity for the determination of electron temperature. A two-temperatures diffusion-dominated plasma model is used to derive the electron temperature from the measured populations of atomic nitrogen levels.

Reprint requests to A. Catherinot, U.E.R. des Sciences Universite d'Orleans, Departement de Physique, *F-45045 Orléans Cedex*, Frankreich.

## II. Experimental Part

### 1. Experimental Set-up

The experimental apparatus is shown schematically in Figure 1. Nitrogen is heated in a plasmatron device which is similar to the one described in Ref. [15]: the electric arc was established between a cone shaped tungsten cathode and a convergent-nozzle copper anode; both electrodes were water-cooled. The electric power was 6 kW and the gas flow rate 5 liter/mn. The plasma formed diffused through the anode exit hole (4 mm in diameter) into an observation chamber (3 cm in diameter, 3 cm long) in which the pressure $P$ was held at a given level in the range $1 < P$(Torr) $< 300$. The gas passed through a heat-exchanger before leaving the device. For the above conditions and running times up to 2 hours, pressure and electric power fluctuations were less than 1% and 3% respectively.

Figure 2* shows photographs of the plasma jet at different pressures in the observation chamber. The bright core that appears for the lowest pressures [$1 < P$(Torr) $< 20$] and which seems to be detached from the main jet, moves towards the anode with increasing pressure and disappears for pressures higher than 20 Torr. In the pressure range $50 < P$ (Torr) $< 150$, the plasma jet is very nearly cylindrical and is not vorticed. All measurements were made in this pressure range because of the very important simplifications of the hydrodynamical equations involved in the theoretical plasma model (see Section III).

* Figure 2 on page 1144 a.

Spectroscopic observations were carried out, through quartz windows, on a plasma cross-section situated 1 mm ahead the anode exit hole. The visible plasma diameter was approximately 3 mm. The quartz windows were cleaned before each run, to minimized light absorption. The spectrograph was a 2 m Hilger-Watts instrument. The spectral lines were observed with a 1200 lines/mm grating in second order yielding 1.27 Å/mm reciprocal dispersion. The spectra were photographically recorded,

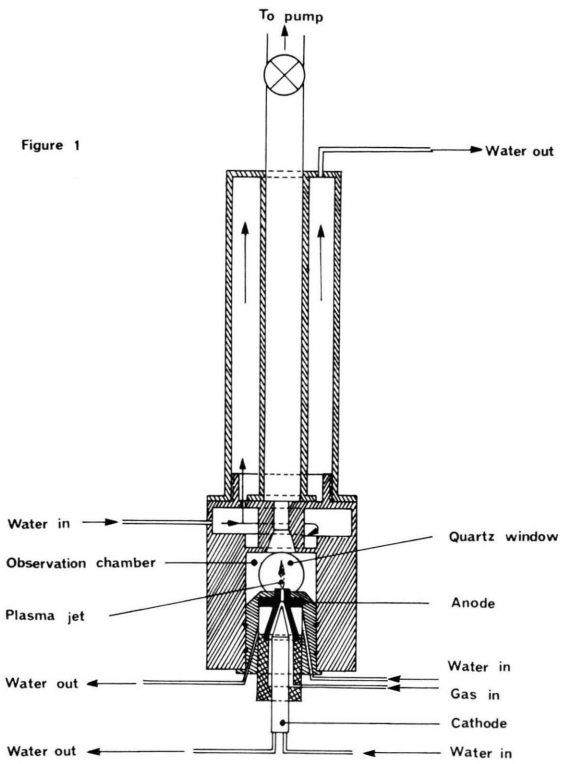


Fig. 1. Schematic drawing of the plasmatron device.

the plates (Kodak 1 N) being calibrated by means of a ribbon tungsten lamp. The external optics between the object and the spectrograph was arranged so that the image on the entrance slit plane was approximately of the same size as the object. Since the radiation observed by the spectrograph was an integral value along a line of sight across the plasma column, Abel inversion [16] was applied in order to obtain the emission coefficient as a function of radial distance.

## 2. Measurements; Results

Two types of measurements have been performed:

1) electron density determination from measured line profile of $\lambda = 4935$ Å atomic nitrogen line,

2) determination of the populations of various electronic states (or, equivalently, excitation temperatures determination) from measurements of selected atomic nitrogen line intensities.

### *a) Electron densities*

Because of the rather small width of $\lambda = 4935$ Å line, an indirect method was used for the purpose of determining electron density distribution in the pure nitrogen plasma. Small amounts of hydrogen were first added to the nitrogen gas and integrated $H_\beta$ line profiles recorded in several planes to both sides of the plasma axis in order to get the data for Abel inversion. The broadening of this line is due almost entirely to Stark effect when the electron density is larger than $10^{14}$ cm$^{-3}$. The relation between electron density and Stark width is known to a good degree of accuracy [17a]. Here, Hill's formula [18] (derived from Griem's results) was used. This formula is:

$$n_e/\mathrm{cm}^{-3} = [C_0(T_e) + C_1(T_e)\log(\Delta\lambda)] \times 10^{13}(\Delta\lambda)^{3/2}, \quad (1)$$

where $\Delta\lambda$ (in Å) is the full half-width of $H_\beta$ line at the radial distance considered; the coefficients $C_0(T_e)$ and $C_1(T_e)$, tabulated by Hill, are very nearly constant in the ranges $10^4 < T_e(^\circ\mathrm{K}) < 4\cdot 10^4$ and $10^{14} < n_e\,(\mathrm{cm}^{-3}) < 10^{17}$.

The atomic nitrogen $\lambda = 4935$ Å line profiles were also measured under identical conditions. It was thus possible to "calibrate" the half widths of this line as a function of $n_e$. The amount of hydrogen was then reduced until the hydrogen partial pressure was zero. It turns out that, for given electric power and total pressure in the observation chamber, the plasma size and geometry were identical for pure nitrogen and for nitrogen-hydrogen mixture. Therefore, provided that the broadening of the $\lambda = 4935$ Å line is due essentially to Stark effect, the electron density $n_e(r)$ of the nitrogen plasma at a radial distance $r$ and the corresponding electron density $n_e^*(r)$ of the nitrogen-hydrogen plasma are related by the simple formula [+]:

$$n_e(r) = n_e^*(r)\, W/W^*,$$

where $W$ and $W^*$ are the widths of the $\lambda = 4935$ Å line for the radial distance considered. To verify

[+] Note that in deriving this formula, assumption is made that the width of an isolated spectral line is proportional to the electron density. This is the case for the electron densities and temperatures encountered in our plasma.

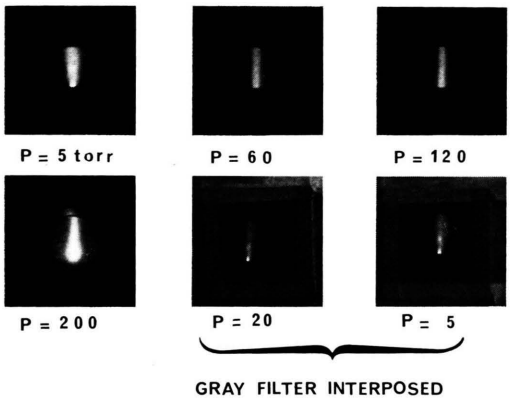


Fig. 2. Typical aspects of the plasma jet.

the above assumption, the ratios $n_e^*/W^*$ obtained were compared to the corresponding ratios taken from Griem [17b]. The agreement was found to be very good.

The electron density distributions so obtained are shown in Fig. 3 for two plasma total pressures. For $P = 120$ Torr, the electron density is nearly constant ($n_e \cong 10^{16}$ cm$^{-3}$) across a radius $r \cong 0.7$ mm and decreases rapidly for larger radial distances. For $P = 60$ Torr, the electron density decreases smoothly from the axial value $n_e(0) \cong 6 \cdot 10^{15}$ cm$^{-3}$.

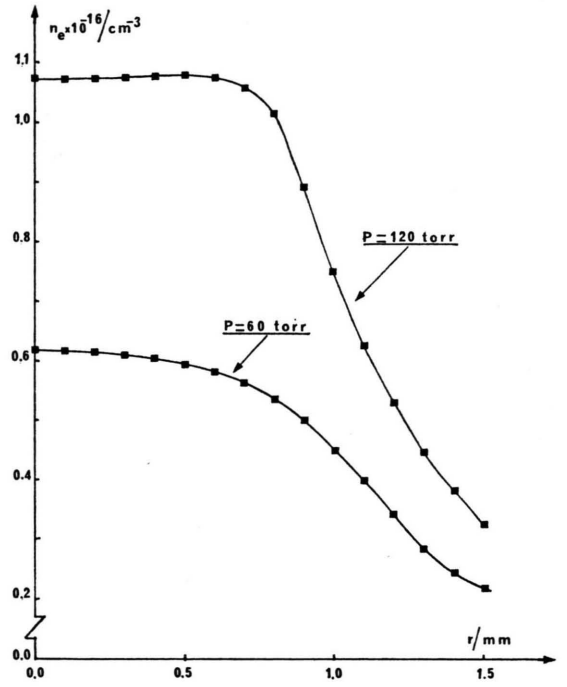


Fig. 3. Radial distribution of the electron density for two different pressures in the observation chamber.

*b) Atomic nitrogen electronic state populations*

The measured nitrogen lines are listed in Table I. These lines were selected for the purpose of providing informations one three types of levels:

1) low lying level ($3p^4S$),
2) intermediate levels ($4p^2S$, $4p^4D$ and $4p^4P$),
3) high lying levels [$2p^2(^1S)3s''^2S$].

The low lying level and the intermediate levels belong to the groups numbered 6 and 11, respectively, in Park's [10] idealized atom nitrogen model (see Sec-

Table I. Atomic parameters of the measured nitrogen lines.

| $\lambda$ (Å) | 7468.31 | 7423.64 | 4935.03 | 4914.90 | 5328.18 | 5281.18 | 5411.88 | 5401.45 |
|---|---|---|---|---|---|---|---|---|
| upper level $i$ | $2p^2(^3P)3p^4S^\circ$ | $2p^2(^3P)3p^4S^\circ$ | $2p^2(^3P)4p^2S^\circ$ | $2p^2(^3P)4p^2S^\circ$ | $2p^2(^3P)4p^4D^\circ$ | $2p^2(^3P)4p^4P^\circ$ | $2p^2(^1S)3s''^2S$ | $2p^2(^1S)3s''^2S$ |
| lower level $j$ | $2p^2(^3P)3s^4P$ | $2p^2(^3P)3s^4P$ | $2p^2(^3P)3s^2P$ | $2p^2(^3P)3s^2P$ | $2s2p^4P$ | $2s2p^4P$ | $2p^2(^3P)3p^2P^\circ$ | $2p^2(^3P)3p^2P^\circ$ |
| $E_i$ (cm$^{-1}$) | 96752 | 96752 | 106479 | 106479 | 106871 | 107039 | 116279 | 116279 |
| $E_j$ (cm$^{-1}$) | 83366 | 83366 | 86221 | 86138 | 88110 | 88110 | 97806 | 97770 |
| $g_i$ | 4 | 4 | 2 | 2 | 8 | 6 | 2 | 2 |
| $g_j$ | 6 | 2 | 4 | 2 | 6 | 6 | 4 | 2 |
| $A_{ij}$ (sec$^{-1}$) * | $0.161 \cdot 10^8$ | $0.052 \cdot 10^8$ | $0.0158 \cdot 10^8$ | $0.759 \cdot 10^6$ | $0.254 \cdot 10^6$ | $0.282 \cdot 10^6$ | $0.75 \cdot 10^6$ | $0.369 \cdot 10^6$ |

* from W. L. Wiese, M. W. Smith, and B. M. Glennon, Atomic transition Probabilities, NSRDS-NBSH (1966).

tion III). Because this classification does not include the ($^1$S) core configuration, the assumption is made here that the $2p^2(^1S)3s''\,^2S$ level ($E_i = 116{,}279$ cm$^{-1}$) is in equilibrium with the close lying ($^3$P) core levels with principal quantum number $n = 11$ ($E_i = 116{,}298$ cm$^{-1}$), i. e. the group of levels numbered 26.

For each line, the radial distribution $\varepsilon_{ij}(r)$ of the emission coefficient per unit volume was obtained by Abel inversion of the measured absolute intensities. The plasma was assumed to be optically thin for the selected lines. Then, the starting level population densities $n_i(r)$ are related to the corresponing emission coefficients by the well-known relation:

$$\varepsilon_{ij} = (h\nu/4\pi)\, n_i A_{ij}\,,$$

where $h$ is the Planck's constant, $\nu$ the central frequency of the line and $A_{ij}$ the transition probability.

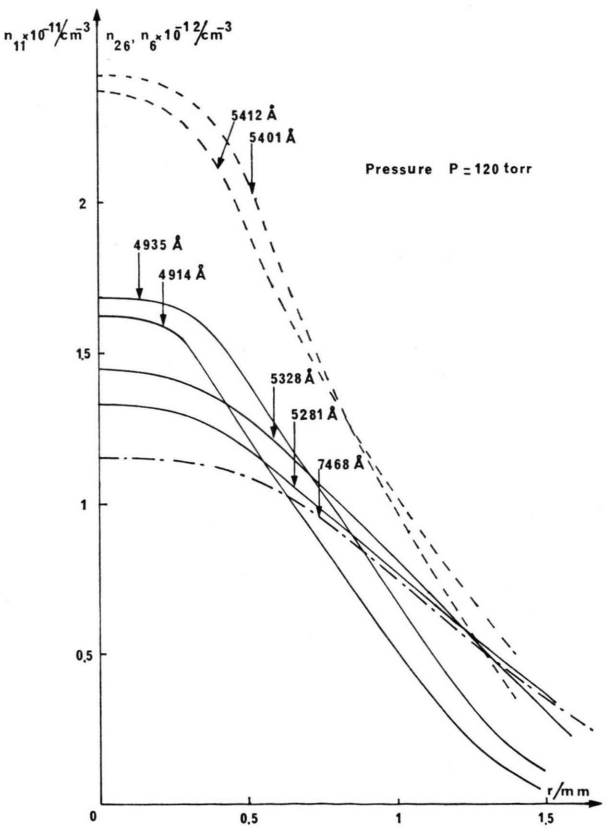


Fig. 4. Measured radial distributions of atomic nitrogen excited state populations for the pressure $P = 120$ Torr
— — — $2p^2$ ($^1$S) $3s''\,^2S$ level (group n° 26),
——— $2p^2$ ($^3$P) $4p\,^2S$, $4p\,^4D$ and $4p\,^4P$ levels (group n° 11),
— · — · $2p^2$ ($^3$P) $3p\,^4S$ level (group n° 6).

Typical results are shown in Figs. 4 and 5. In Fig. 4, the radial distribution of population densities are presented; in Fig. 5, the functions $\ln(n_i/g_i)$, where $g_i$ is the statistical weight of level $i$, are plotted versus the energy $E_i$ for different radial distances. It turns out that $\ln(n_i/g_i)$ is not a linear function of the energy. Consequently, the electronic excitation temperatures derived from these graphs depend on the groups of levels considered as shown in Fig. 6 for two working pressures. On the other hand, due to the relatively high electron density in the plasma, the highest lying levels were expected to be in partial LTE with the electrons[+]. The Saha temperature distributions resulting from this assumption for the group of levels $i = 11$ ($E_\infty - E_{11} \cong 10{,}000$ cm$^{-1}$) are displayed in Figure 6. It is observed that the Saha temperature so obtained is everywhere higher than the electronic excitation temperature derived from the ratio of populations of group 11 and group 26 ($E_\infty - E_{26} \cong 1{,}000$ cm$^{-1}$). Note also that the Saha temperature exibits an off-axis maximum at approximately $r \sim 0{,}8$ mm in both cases.

From the above experimental results it follows that the true electron temperature is given neither by the Boltzmann plot nor by the ratio of two levels populations (even if these levels are situated relatively high in the energy scale). Consequently, a non-LTE plasma model is necessary in order to derive the true electron temperature.

## III. Non-LTE Plasma Model

### 1. Rate Equations

In an ionized gas, the relaxation times for the translational energy between the electrons and the heavy particles are much larger than the corresponding relaxation times inside each particles group. Therefore, the plasma can assumed to be a mixture of two weakly interacting fluids [20, 21]: electrons on the one hand, heavy particles on the other hand. The heavy particles contribution to the transport properties of the plasma does practically not depend on the electrons and can be calculated by classical

[+] According to Drawin's LTE criterion [19] for a stationary homogeneous plasma, the levels with principal quantum number $n > 3$ are in partial LTE with the electrons when $n_e > 10^{14}$ cm$^{-3}$ for the temperature range of interest. This condition is fulfilled here but the plasma is inhomogeneous.

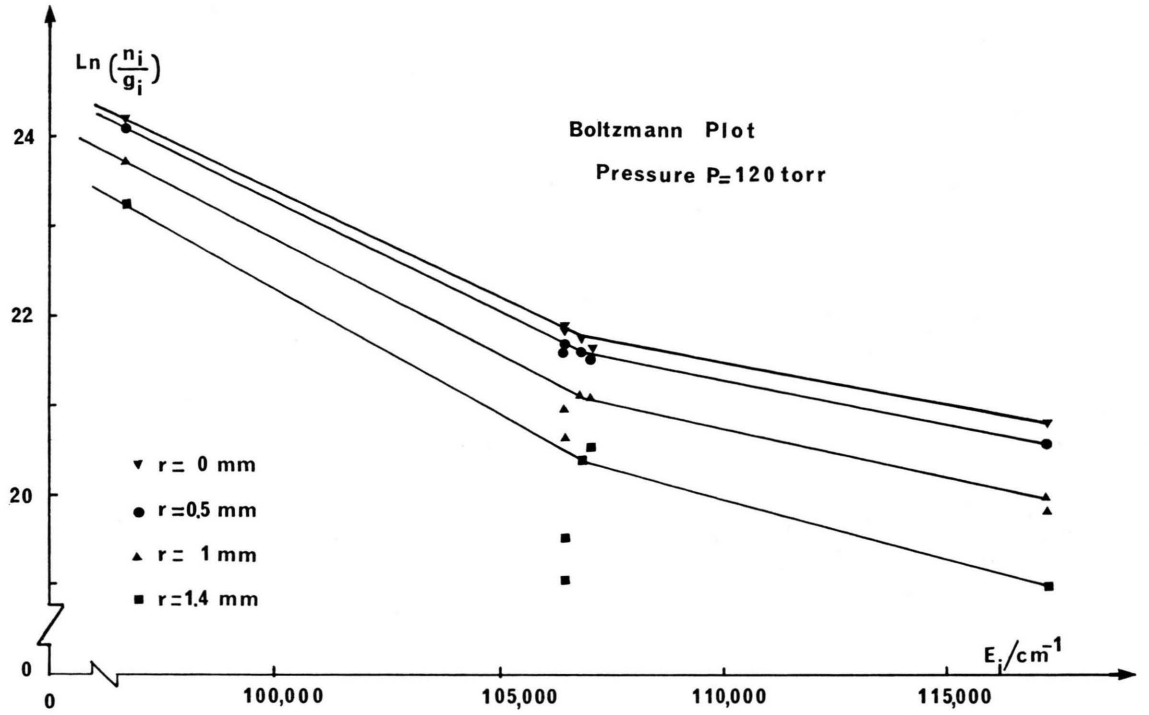


Fig. 5. Boltzmann plot of the population densities $n_i/g_i$ at various radial distances and for the pressure $P = 120$ Torr.

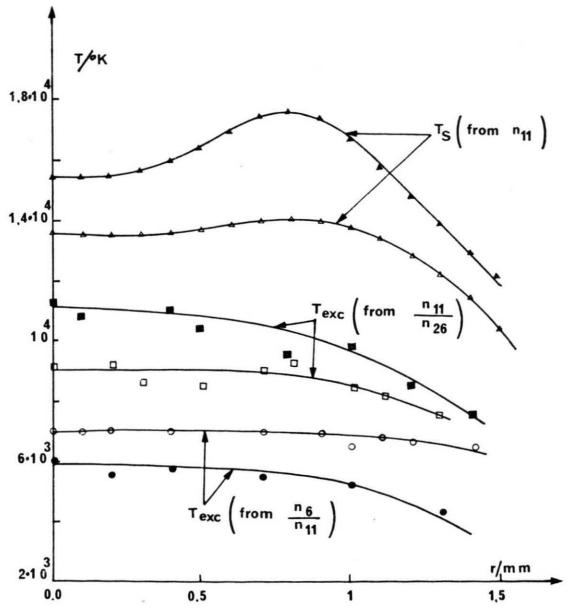


Fig. 6. Electronic excitation temperatures ($T_{exc}$) and Saha temperature ($T_S$) obtained from the measured populations; ▲, ■, ● $P = 120$ Torr; △, □, ○ $P = 60$ Torr.

methods [22, 23]. Besides, in a sufficiently ionized and collision-dominated plasma, it have been shown [20, 21, 24] that the electrons and heavy particles have (to zero order approximation) the same mean hydrodynamical velocity $\langle \boldsymbol{v}_0 \rangle$ but maxwellian velocity distributions in a frame moving with the velocity $\langle \boldsymbol{v}_0 \rangle$. Due to the specific character of the plasma considered here (see Section II), $\langle \boldsymbol{v}_0 \rangle$ is everywhere parallel to the plasma axis and has a negligible gradient in this direction. Under these conditions, the following assumptions can be made:

1) the plasma is cylindrical, axial gradients being negligible in comparison with radial gradients;
2) the plasma is stationary, quasi-neutral, field-free and consists of electrons, singly charged atomic nitrogen ions in their ground state and neutral nitrogen atoms [+]:
3) the plasma is of sufficient density so that collisional transition rates are much larger than radiative transition rates (collision-dominated plasma);

[+] The study is limited to the plasma jet core, i. e. to the region where it is expected that $N_2$ and $N_2^+$ densities are negligibly small compared to atomic species densities (see concluding remarks of Section III).

4) the electrons and heavy particles have maxwellian velocity distributions at temperatures $T_e$ and $T_h$, respectively, which may be different.

The population density $n_i$ of a bound atomic level $i$ is then given by the relation [12, 25]:

$$\nabla_r \cdot (n_i \langle \boldsymbol{V}_i \rangle) = (\partial n_i/\partial t)_{\substack{\text{coll.,} \\ \text{rad.}}} \quad (4)$$

where $\langle \boldsymbol{V}_i \rangle$ is the mean diffusion velocity of atoms in state $|i\rangle$. The calculations are based on an idealized atomic nitrogen model given by Park [10]: the individual energy levels are grouped into 35 group of levels (here "$i$" denotes the serial number of the group of levels considered). Since collisions between heavy particles are inefficient in causing the transition of electrons between bound states and between free and bound states, the only collision and radiative processes taken into account are:

- collisional ionization and three-body recombination

$$N_i + e \underset{K_{\infty i}}{\overset{K_{i\infty}}{\rightleftarrows}} N^+ + e + e;$$

- collisional excitation and de-excitation

$$N_i + e \underset{K_{ji}}{\overset{K_{ij}}{\rightleftarrows}} N_j + e;$$

- photo-ionization and radiative recombination

$$N_i + h\nu \underset{\beta_i}{\overset{\beta_i(1-\Lambda_i)}{\rightleftarrows}} N^+ + e;$$

- photo-absorption and spontaneous emission

$$N_i + h\nu_{ji} \underset{A_{ji}}{\overset{A_{ji}(1-\Lambda_{ji})}{\rightleftarrows}} N_j .$$

In the above notation, $N$ represents a neutral nitrogen atom, $N^+$ its associated ion and e a free electron; the subscripts $i$ and $j$ denote two different bound atomic states and $\infty$ the ionized state; $\Lambda_i$ and $\Lambda_{ji}$ are optical escape factors and account for radiative reabsorption [25]; $K$, $\beta$ and $A$ are rate coefficients for the indicated processes.

The radiative transition probabilities $A_{ji}$ are taken from Wiese, Smith and Glennon [26]; the other rate coefficients are calculated as follows:

i) collisional ionization rate coefficients $K_{i\infty}$: For the levels $2p^3(^4S)$, $2p^3(^2D)$ and $2p^3(^2P)$ we used the ionization cross-sections given by Lotz [27], for all other levels Drawin's formula [28] was applied. We found that, when the temperature range is limited to $8 \cdot 10^3 < T(^\circ K) < 2 \cdot 10^4$, the rate coefficients $K_{i\infty}$ can be approximated (with a precision of 10% or better) by the formula:

$$K_{i\infty} = \exp\{X_i + Y_i \exp(Z_i T_e)\}. \quad (5)$$

The coefficients $X_i$, $Y_i$ and $Z_i$ are listed in Table II. The collisional recombination rate coefficients $K_{\infty i}$ are derived from the $K_{i\infty}$ by the detailed balance relation [+]:

$$n_i^s K_{i\infty} = n_e K_{\infty i}, \quad (6)$$

where $n_i^s$ is the Saha density:

$$n_i^s = n_e^2 \frac{g_i}{2Z^+} \left(\frac{h^2}{2\pi m_e k T_e}\right)^{3/2} \exp\left\{\frac{E_{i\infty}}{k T_e}\right\}. \quad (7)$$

In the above relation, $n_e$ is the electron density, $g_i$ the statistical weight of level $i$, $Z^+$ the partition function of singly charged atomic nitrogen ions, $h$ the Planck's constant, $k$ the Boltzmann's constant, $m_e$ the electron mass and $E_{i\infty} = E_\infty - E_i$ the effective ionization energy of level $i$ ($E_\infty = 117{,}214\ cm^{-1}$ for atomic nitrogen).

ii) Collisional transition rate coefficients $K_{ij}$: We used an approximation given by Park [10, 29]:

$$K_{ij} = \frac{C_{ij}(T_e/10^4)^{m_{ij}} g_j}{\bar{n}_i^5 \bar{n}_j^5 (1/\bar{n}_i^2 - 1/\bar{n}_j^2)^4} \exp\left\{\frac{(E_j - E_i)}{k T_e}\right\} \quad (8)$$

where $\bar{n}_i$ is the effective principal quantum number of level $i$ ($\bar{n}_i = (E_1^H/E_{i\infty})^{1/2}$, $E_1^H$ ionization energy of hydrogen atom) and $C_{ij}$ and $m_{ij}$ are coefficients listed in Reference [10]. Nevertheless, for $i, j = 1, 2, 3$ the coefficients $C_{ij}$ and $m_{ij}$ have been calculated in the present work using Smith, Henry, and Burke's [30] cross-section instead of Gryzinski's results used by Park.

The de-excitation rate coefficients $K_{ji}$ are derived from the corresponding excitation rate coefficients by the detailed balance relation:

$$n_i^s K_{ij} = n_j^s K_{ji}. \quad (9)$$

iii) Radiative recombination rate coefficients $\beta_i$: The rate coefficients $\beta_i$ have been calculated from the photoabsorption coefficients $\alpha_{i\infty}$. For levels with principal quantum number $n > 4$, we used the Kramers-Unsöld Eq. for $\alpha_{i\infty}$ multiplied by Gaunt factors given by Karzas and Latter [31]. For levels with $n = 3$, the calculation was

[+] Note that $K_{i\infty}$ and $K_{\infty i}$ have the same dimensions, since $K_{\infty i}$ contains the electron density.

Table II. Coefficients of proposed approximations for the ionization rate coefficient $K_{i\infty}$ and radiative recombination rate coefficient $\beta_i$ in the temperature range $8{,}000 < T_e$ (°K $< 20{,}000$; $K_{i\infty}$ and $\beta_i$ are in $cm^3\,sec^{-1}$ and numbers following E denote power of ten by which the numbers are to be multiplied.

| Level no $i$ | Coefficients appearing in Eq. (5) for $K_{i\infty}$ ($cm^3\,s^{-1}$) $X_i$ | $Y_i$ | $Z_i$ | Coefficients appearing in Eq. (10) for $\beta_i$ ($cm^3\,s^{-1}$) $A_i$ | $B_i$ | $C_i$ |
|---|---|---|---|---|---|---|
| 1 | −2.82 E+01 | −8.52 E+01 | −2.24 E−04 | −4.05 E−22 | −2.27 E−18 | 5.52 E−13 |
| 2 | −2.66 E+01 | −7.42 E+01 | −2.24 E−04 | −1.90 E−22 | +1.08 E−17 | −4.43 E−14 |
| 3 | −2.57 E+01 | −6.81 E+01 | −2.23 E−04 | −3.43 E−23 | 1.52 E−18 | −9.39 E−15 |
| 4 | −1.87 E+01 | −2.32 E+01 | −2.13 E−04 | −1.84 E−24 | 4.11 E−20 | +2.13 E−16 |
| 5 | −1.83 E+01 | −2.14 E+01 | −2.12 E−04 | 9.73 E−24 | −6.61 E−19 | 2.19 E−14 |
| 6 | −1.69 E+01 | −1.56 E+01 | −2.08 E−04 | 3.94 E−23 | −1.69 E−18 | 3.17 E−14 |
| 7 | −1.66 E+01 | −1.46 E+01 | −2.07 E−04 | 1.61 E−23 | −7.95 E−19 | 1.90 E−14 |
| 8 | −1.52 E+01 | −1.02 E+01 | −2.04 E−04 | 3.47 E−23 | −1.22 E−18 | 1.52 E−14 |
| 9 | −1.49 E+01 | −9.55 E+00 | −2.03 E−04 | 1.59 E−22 | −7.31 E−18 | 1.23 E−13 |
| 10 | −1.49 E+01 | −9.52 E+00 | −2.03 E−04 | 7.88 E−23 | −3.64 E−17 | 6.15 E−14 |
| 11 | −1.44 E+01 | −8.10 E+00 | −2.02 E−04 | 1.34 E−22 | −4.71 E−18 | 5.73 E−14 |
| 12 | −1.36 E+01 | −6.24 E+00 | −2.05 E−04 | 1.71 E−23 | −5.97 E−19 | 7.02 E−15 |
| 13 | −1.34 E+01 | −5.99 E+00 | −2.05 E−04 | 3.12 E−22 | −1.09 E−17 | 1.28 E−13 |
| 14 | −1.34 E+01 | −5.87 E+00 | −2.05 E−04 | 4.48 E−22 | −1.56 E−17 | 1.83 E−13 |
| 15 | −1.31 E+01 | −5.27 E+00 | −2.07 E−04 | 6.24 E−23 | −2.17 E−18 | 2.49 E−14 |
| 16 | −1.25 E+01 | −4.31 E+00 | −2.12 E−04 | 1.01 E−23 | −3.46 E−19 | 3.83 E−14 |
| 17 | −1.25 E+01 | −4.19 E+00 | −2.13 E−04 | 1.36 E−22 | −4.69 E−18 | 5.18 E−14 |
| 18 | −1.24 E+01 | −4.10 E+00 | −2.14 E−04 | 4.47 E−22 | −1.53 E−17 | 1.69 E−12 |
| 19 | −1.22 E+01 | −3.77 E+00 | −2.17 E−04 | 3.53 E−23 | −1.20 E−18 | 1.30 E−14 |
| 20 | −1.17 E+01 | −3.11 E+00 | −2.25 E−04 | 7.33 E−22 | −2.46 E−18 | 2.56 E−14 |
| 21 | −1.17 E+01 | −3.08 E+00 | −2.26 E−04 | 4.00 E−22 | −1.34 E−17 | 1.39 E−13 |
| 22 | −1.13 E+01 | −2.51 E+00 | −2.39 E−04 | 4.33 E−22 | −1.43 E−17 | 1.43 E−13 |
| 23 | −1.08 E+01 | −2.01 E+00 | −2.59 E−04 | 3.53 E−22 | −1.14 E−17 | 1.11 E−13 |
| 24 | −1.04 E+01 | −1.66 E+00 | −2.87 E−04 | 2.87 E−22 | −9.19 E−18 | 8.67 E−14 |
| 25 | −1.01 E+01 | −1.44 E+00 | −3.27 E−04 | 2.34 E−22 | −7.42 E−18 | 6.87 E−14 |
| 26 | −9.84 E+00 | −1.39 E+00 | −3.94 E−04 | 1.91 E−22 | −6.02 E−18 | 5.49 E−14 |
| 27 | −9.58 E+00 | −1.42 E+00 | −4.82 E−04 | 1.58 E−22 | −4.93 E−18 | 4.45 E−14 |
| 28 | −9.35 E+00 | −1.32 E+00 | −5.90 E−04 | 1.31 E−22 | −4.07 E−18 | 3.64 E−14 |
| 29 | −9.13 E+00 | −5.79 E−02 | −4.73 E−04 | 1.09 E−22 | −3.40 E−18 | 3.02 E−14 |
| 30 | −8.98 E+00 | +1.24 E−01 | −8.00 E−05 | 9.19 E−23 | −2.84 E−18 | 2.51 E−14 |
| 31 | −8.60 E+00 | −8.04 E−02 | +5.07 E−05 | 7.78 E−23 | −2.40 E−18 | 2.11 E−14 |
| 32 | −8.39 E+00 | −9.53 E−02 | +5.37 E−05 | 6.62 E−23 | −2.04 E−18 | 1.79 E−14 |
| 33 | −8.08 E+00 | −2.20 E−01 | 3.46 E−05 | 5.70 E−23 | −1.75 E−18 | 1.53 E−14 |
| 34 | −7.42 E+00 | −7.10 E−01 | 1.53 E−05 | 4.92 E−23 | −1.51 E−18 | 1.32 E−14 |
| 35 | −2.67 E+01 | +1.87 E+01 | −7.73 E+07 | 4.28 E−23 | −1.31 E−18 | 1.14 E−14 |

based on Griem's cross-sections [17c]. For levels $2p^3(^4S)$, $2p^3(^2D)2p^3(^2P)$, we used the $\alpha_{i\infty}$ values listed by Peach [32]. Especially for the $2p^3(^4S)$ term, the Peach's data have been extended by those of Bates and Estermann [33] (which were obtained from experimental results of Samson and Cairns [34]). Fast decrease of $\alpha_{i\infty}$ below $\lambda = 852$ Å is assumed for the $2p^3(^2D)$ term and the absorption peaks at $\lambda = 963$ Å and $\lambda = 852$ Å are taken into account for the $2p^3(^2P)$ term. As for collisional ionization rate coefficients, we found that the $\beta_i$ can be approximated (in the temperature range considered) by the simple formula:

$$\beta_i = A_i T_e^2 + B_i T_e + C_i . \tag{10}$$

The coefficients $A_i$, $B_i$ and $C_i$ are listed in Table II. (Note that these coefficients are partly positive and partly negative.)

Under the foregoing conditions, the bound state population densities of nitrogen atom obey the following equations [25]:

$$\frac{1}{r}\frac{d}{dr}(r\, n_i \langle V_i \rangle) = -n_e n_i K_{i\infty} + \sum_{\substack{j \\ j \neq i}} K_{ij} + \frac{1}{n_e}\sum_{\substack{j \\ j<i}} A_{ij} \Lambda_{ij} + n_e\left(\sum_{\substack{j \\ j \neq i}} n_j K_{ji} + \frac{1}{n_e}\sum_{\substack{j \\ j>i}} n_j A_{ji} \Lambda_{ij}\right) + n_e^2 (K_{\infty i} + \beta_i \Lambda_i) , \tag{11}$$

subject to the conservation condition:

$$n_a = \sum_{i=1}^{p} n_i = \sum_{i=1}^{p} b_i n_i^s , \tag{12}$$

where $n_a$ is the total atom density, $p$ the total number of bound electronic states and $b_i = n_i/n_i^s$ the Saha decrement. The $(p+1)$ coupled Eqs. (11) and (12) can be put into the form [10, 35]:

$$F \cdot b = G + x H \tag{13}$$

where (1) $F$ is a matrix whose elements $F_{ij}$ (functions only of $n_e$, $T_e$ and $\Lambda_{ij}$) are

– for $i = p+1$: $F_{p+1,j} = n_j^s/n_e^2$;

– for $i \leqq p$:

$$F_{ii} = -\left[K_{i\infty} + \sum_{\substack{j \\ j \neq i}} K_{ij} + \frac{1}{n_e} \sum_{\substack{j \\ j<i}} A_{ij}\Lambda_{ij}\right]$$

$$F_{ij} = \begin{cases} \dfrac{n_j^s}{n_i^s} K_{ij}, & \text{if } j<i; \\ K_{ij} + \dfrac{1}{n_e}\dfrac{n_j^s}{n_i^s} A_{ij}\Lambda_{ji}, & \text{if } j>i; \end{cases}$$

(2) $b$ is a vector whose components $b_i$ are the Saha decrements;

(3) $G$ is a vector whose components $G_i$ are:

· for $i = p+1$: $G_i = 0$;

· for $i \leqq p$:

$$G_i = -\frac{n_e}{n_i^s}(K_{\infty i} + \beta_i \Lambda_i) + \frac{1}{n_e n_i^s}\frac{1}{r}\frac{d}{dr}(r\, n_i \langle V_i \rangle);$$

(4) $x$ is a nonequilibrium parameter (function of $n_e$, $T_e$ and $n_a$) defined by the ratio:

$$x = n_a/n_a^s \tag{14}$$

where $n_a^s$ is the total Saha density:

$$n_a^s = \sum_{i=1}^{p} n_i^s = n_e^2 \frac{Z_a}{2Z^+}\left(\frac{h^2}{2\pi m_e k T_e}\right)^{3/2} \exp\left\{\frac{E_\infty}{k T_e}\right\}, \tag{15}$$

$Z_a$: partition function of neutral nitrogen atoms.

(5) $H$ is a vector of components $H_i = 0$ for $i \leqq p$ and

$$H_{p+1} = n_a^s/n_e^2.$$

## 2. General Numerical Results

In the following we assume that the plasma is optically thin for the free-bound continua, i. e. we put $\Lambda_i = 1$ (which is fulfilled under most experimental conditions). The foregoing system of equations is solved for different given values of $n_e$, $T_e$, $\Lambda_{ij}$ and for two idealized physical situations.

### *a) Homogeneous Stationary Plasma*

In this case, the left hand sides of Eq. (11) vanish, since no diffusion takes place. Numerical results are given here for two different cases of optical reabsorption and for $x = 1$. It must be emphasis that only slight deviations from Saha-Boltzmann populations can occur in a homogeneous stationary plasma when $n_a = n_a^s$. Practically, all $n_i$ must be close to unity whatever be the electron density.

i) Optically thin case: no reabsorption occurs, i. e. all escape factors $\Lambda_{ij}$ are equal to unity. Table III presents the Saha decrements $b_i$ obtained for an electron temperature $T_e = 12{,}000\ ^\circ\mathrm{K}$ and different electron densities. At low electron densities ($n_e < 10^{15}\ \mathrm{cm}^{-3}$), the first excited levels (especially the $3s(^4P)$ and $3s(^2P)$ states) are slightly underpopulated ($b_i < 1$) while the levels for which $E_{i\infty} \lesssim 2{,}300\ \mathrm{cm}^{-1}$ are in partial LTE with the electrons. At high electron densities ($n_e > 10^{15}\ \mathrm{cm}^{-3}$), all levels are populated according to the Saha-Boltzmann distribution, radiation escape has a negligible effect.

The influence of the electron temperature is shown in Figure 7. For a given electron density, one sees that the departure from LTE populations of the first excited levels decreases with increasing electron temperature. The results are in agreement with those obtained in hydrogen and helium [11, 12, 25].

ii) Optically thick resonance radiation case: complete reabsorption of the resonance multiplets $2p^2(^3P)3s$, $2p^2(^3P)3d$ and $2p^2(^3P)4s$ is assumed, the plasma being optically thin for all other photons. Computed Saha decrements $b_i$ are presented in Table III for an electron temperature $T_e = 12{,}000\ ^\circ\mathrm{K}$ and different electron densities. In this case, alle excited states are very nearly in equilibrium with the electrons for $n_e > 10^{14}\ \mathrm{cm}^{-3}$ in good agreement with Drawin's LTE conditions [19].

### *b) Inhomogeneous Stationary Plasma*

The plasma is now assumed to be strongly inhomogeneous. As stated by Drawin and Emard [11], when the smallest plasma dimension $d$ in direction

Table III. Saha decrements $b_i = n_i/n_i^S$ for a stationary homogeneous nitrogen plasma with $T_e = 12{,}000\,°K$ and $x = n_a/n_a^S = 1$.

| | Optically thin | | | | Optically thick resonance radiation | | | | |
|---|---|---|---|---|---|---|---|---|---|
| $n_e$ (cm$^{-3}$) | | | | | $n_e$ (cm$^{-3}$) | | | | |
| $i$ | $10^{13}$ | $10^{14}$ | $10^{15}$ | $10^{16}$ | $i$ | $10^{13}$ | $10^{14}$ | $10^{15}$ | $10^{16}$ |
| 1 | 0.98 | 1.00 | 1.00 | 0.99 | 1 | 0.98 | 1.00 | 1.00 | 1.00 |
| 2 | 1.05 | 1.01 | 1.00 | 1.05 | 2 | 1.05 | 1.00 | | |
| 3 | 1.09 | 1.02 | 1.00 | 1.04 | 3 | 1.09 | 1.01 | | |
| 4 | 0.04 | 0.22 | 0.74 | 0.98 | 4 | 1.71 | 1.06 | | |
| 5 | 0.05 | 0.27 | 0.77 | 0.98 | 5 | 1.46 | 1.04 | | |
| 6 | 0.40 | 0.52 | 0.84 | 0.99 | 6 | 1.12 | 1.00 | | |
| 7 | 0.42 | 0.63 | 0.89 | 0.99 | 7 | 0.88 | 0.97 | | |
| 8 | 0.57 | 0.82 | 0.95 | 1.00 | 8 | 0.67 | 0.95 | | |
| 9 | 0.71 | 0.82 | 0.94 | | 9 | 0.91 | 0.98 | | |
| 10 | 0.50 | 0.80 | 0.94 | | 10 | 0.63 | 0.93 | | |
| 11 | 0.79 | 0.88 | 0.96 | | 11 | 0.90 | 0.98 | | |
| 12 | 0.93 | 0.95 | 0.98 | | 12 | 0.98 | 0.99 | | |
| 13 | 0.92 | 0.94 | 0.98 | | 13 | 0.98 | 0.99 | | |
| 14 | 0.90 | 0.93 | 0.98 | | 14 | 0.97 | 0.99 | | |
| 15 | 0.94 | 0.96 | 0.99 | | 15 | 0.99 | 0.99 | | |
| 16 | 0.97 | 0.97 | 1.00 | | 16 | 1.00 | 1.00 | | |
| 17 | 0.97 | 0.97 | | | 17 | | | | |
| 18 | 0.96 | 0.96 | | | 18 | | | | |
| 19 | 0.97 | 0.97 | | | 19 | | | | |
| 20 | 0.98 | 0.98 | | | 20 | | | | |
| 21 | 0.98 | 0.98 | | | 21 | | | | |
| 22 | 1.00 | 1.00 | | | 22 | | | | |
| 23 | | | | | 23 | | | | |
| ⋮ | | | | | ⋮ | | | | |
| 35 | | | | | 35 | | | | |

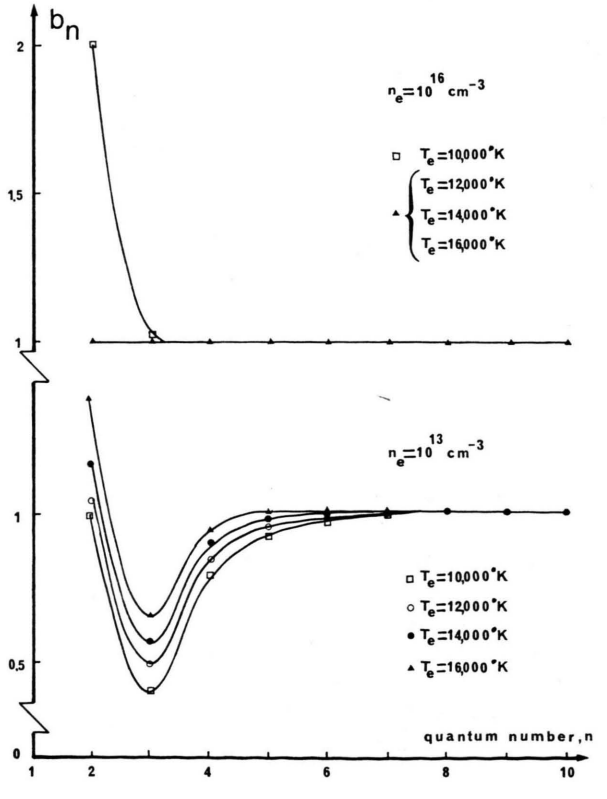


Fig. 7. Averaged Saha decrement $b_n$ as a function of principal quantum number $n$ for a stationary, homogeneous and optically thin nitrogen plasma with $x = n_a/n_a^S = 1$; $b_n$ is an average of the Saha decrements $b_i = n_i/n_i^S$ relative to all levels with a principal quantum number $n$.

of the gradients is larger than the diffusion length $\lambda_{i<1}$ of particles in excited states and when the conditions

$$\left|\frac{T_e(d+\lambda_{i>1}) - T_e(d)}{T_e(d)}\right| \ll 1\,,$$

$$\left|\frac{n_e(d+\lambda_{i>1}) - n_e(d)}{n_e(d)}\right| \ll 1$$

are fulfilled, the excited particles can be assumed in a quasi-steady state with respect to the electrons and to the ground state particles, whereas the ground state particles can still deviate from the quasi-steady state populations, since $\lambda_1 \gg \lambda_i$. For the type of plasma considered here, these conditions are fulfilled. Accordingly, the left hand sides of Eqs. (11) vanish for all states but the three equivalent ground states $2p^3(^4S)$, $2p^3(^2D)$ and $2p^3(^2P)$. Furthermore, the relative contribution of these three states to the diffusion of the neutrals can be assumed to satisfy

Boltzmann distribution, owing to the small energy gap between these three states. One has then:

$$\left(\frac{\partial n_a}{\partial t}\right)_{\substack{\text{coll.}\\ \text{rad.}}} \simeq \sum_{i=1}^{3}\left(\frac{\partial n_i}{\partial t}\right)_{\substack{\text{coll.}\\ \text{rad.}}} = \sum_{i=1}^{3}\frac{1}{r}\frac{\mathrm{d}}{\mathrm{d}r}\left(r\, n_i \langle V_i\rangle\right) \cong -\left(\frac{\partial n_e}{\partial t}\right)_{\substack{\text{coll.}\\ \text{rad.}}}$$

where

$$\left(\frac{\partial n_e}{\partial t}\right)_{\substack{\text{coll.}\\ \text{rad.}}} = n_e \sum_{i=1}^{p}\left[n_i K_{i\infty} - n_e K_{\infty i} - n_e \beta_i\right] . \quad (17)$$

Equations (17) can be put into the form [10]:

$$\left(\frac{\partial n_e}{\partial t}\right)_{\substack{\text{coll.}\\ \text{rad.}}} = k_f n_e n_a - k_r n_e^3 - \alpha n_e^2 \quad (18)$$

where $k_f$, $k_r$ and $\alpha$ are the global rate coefficient for collisional ionization, collisional recombination and radiative recombination, respectively: $\alpha = \sum_{i=1}^{p}\beta_i$ is a function of electron temperature only; in the case of a collision-dominated plasma, $k_f$ and $k_r$ are also functions of electron temperature only and are related by the Saha function

$$k_f = (n_e^2/n_a^s)\, k_r \quad (19)$$

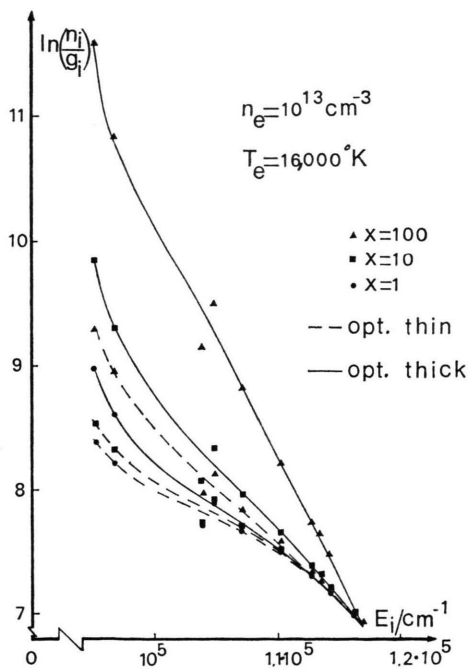


Fig. 8. Boltzmann plot of population densities for a stationary inhomogeneous nitrogen plasma with $n_e = 10^{13}\,\mathrm{cm}^{-3}$ and $T_e = 16{,}000\,^\circ\mathrm{K}$.

and, as shown by Park [36], $k_r$ can be approximated by the simple formula:

$$k_r = 1.15 \times 10^{-26} (T_e/10^4)^{-5.27}\ (\mathrm{cm}^6\,\mathrm{sec}^{-1}) . \quad (20)$$

By substituting Eqs. (18) and (19) into Eq. (16), one has [+]:

$$\sum_{i=1}^{3}\left(\frac{\partial n_i}{\partial t}\right)_{\substack{\text{coll.}\\ \text{rad.}}} = -k_r(x-1)\, n_e^3 + \alpha n_e^2 . \quad (21)$$

Using Eq. (21) and approximation (16), the components of the vector $G$ in (13) can be computed for any given values of $T_e$, $n_e$ and $x$.

Figures 8 and 9 present the variation of $\ln(n_i/g_i)$ as function of the energy $E_i$ for $T_e = 16{,}000\,^\circ\mathrm{K}$, two electron densities and three $x$ values. Optically thin case and optically thick resonance radiation case are both considered in these figures (for $n_e = 10^{16}\,\mathrm{cm}^{-3}$, optically thin and optically thick cases give the same result for each $x$ value since the system is practically collision-dominated).

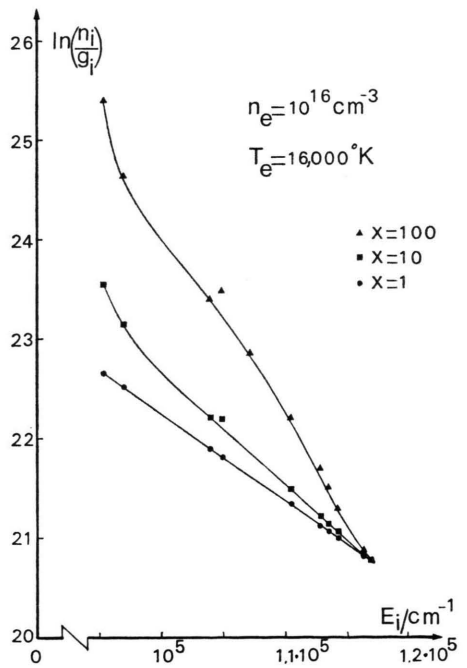


Fig. 9. Boltzmann plot of population densities for a stationary inhomogeneous nitrogen plasma with $n_e = 10^{16}\,\mathrm{cm}^{-3}$ and $T_e = 16{,}000\,^\circ\mathrm{K}$. Optically thin and optically thick resonance radiation cases give the same result for each value of the nonequilibrium parameter $x = n_a/n_a^S$.

[+] Note that $x$ can be much larger than unity when the total plasma pressure $P = n_e k T_e + (n_e + x n_a^s) k T_h$ is constant and $T_e > T_h$. For instance, when $P = 120$ Torr, $T_e = 1.4 \times 10^4\,^\circ\mathrm{K}$, $T_h = 10^4\,^\circ\mathrm{K}$ and $n_e = 10^{16}\,\mathrm{cm}^{-3}$, one has $x \sim 76$.

It turns out that the high lying levels, i. e. the levels above 105,000 $cm^{-1}$, are on a straight line whatever be the electron density and the nonequilibrium parameter, but the slope of each curve does not represent the electron temperature, which means that even highly excited states are not populated according to electron temperature. For $n_e = 10^{16}$ $cm^{-3}$ and $x = 100$, the slope gives an electronic excitation temperature of 6,700 °K which is appreciably lower than the electron temperature of 16,000 °K used for the computation: the excited states are overpopulated due to diffusion processes only, since the radiation escape has a negligible effect. For $n_e = 10^{13}$ $cm^{-3}$ and $x = 100$, the slope gives an electronic excitation temperature of 7,500 °K in the optically thick case, which is again lower than the electron temperature, and of 15,500 °K in the optically thin case, which is close to the electron temperature. Thus, at a low electron density, the radiation escape balances partly the effects of diffusion processes on excited state populations.

## 3. Application to the Present Measurements

Since the electron density distribution is known from experiment, Eq. (13) can be solved for given values of the electron temperature $T_e$ and the nonequilibrium parameter $x = n_a/n_a^S$ in order to get the electronic state populations. The most probable values of $T_e$ and $x$ are those which give the best agreement between computed and measured populations for each radial distance $r$. The results so obtained are shown in Fig. 10 as triangles for $T_e(r)$ and as squares for $x(r)$.

Now, the electron temperature $T_e$ must satisfy also the electron energy equation, namely the equation [20, 37, 38]:

$$(S_e)_{\substack{\text{coll.}\\ \text{rad.}}} = \nabla_r \cdot \left(\tfrac{5}{2} k T_e \boldsymbol{g}_e - \lambda_e \nabla_r T_e\right), \quad (22)$$

where $\lambda_e$ is the thermal conductivity of electrons and $\boldsymbol{g}_e$ the ambipolar diffusion flux. When the variation with the temperature and its gradient is neglected, $g_e$ is given by the relation [37, 39]:

$$g_e = n_e \langle V_{amb} \rangle = -\frac{n^2 m_h}{\varrho} D_A \frac{d}{dr}\left(\frac{n_e}{n}\right) \quad (23)$$

where $n = n_e + n_a + n_+ = 2 n_e + n_a$, $m_h$ is the atomic nitrogen mass, $D_A$ the ambipolar diffusion coefficient and $\varrho$ the plasma density.

The left hand side of Eq. (22) is calculated on the basis of the collisional-radiative model given above. The electron energy equation can then be put into the form:

$$2 n_e \frac{m_e}{m_h} \sum_{\substack{q \\ q=i,+}} \bar{\nu}_{eq} \left[\tfrac{3}{2} k (T_h - T_e)\right] - n_e^2 \sum_i \beta_i (E_\infty + \tfrac{3}{2} k T_e - E_i) + E_\infty \left(\frac{\partial n_e}{\partial t}\right)_{\substack{\text{coll.}\\ \text{rad.}}} = \frac{1}{r} \frac{d}{dr} \tfrac{5}{2} k T_e r g_e - \lambda_e r \left(\frac{dT_e}{dr}\right), \quad (24)$$

where $\bar{\nu}_{eq}$ is the collision frequency between a heavy particle (atom on the state $i$ or singly charged atomic ion) and an electron. In addition, the electron and heavy particle temperatures must verify the equation of state:

$$P = n_e k T_e + (n_e + n_a) k T_h, \quad (n_+ = n_e). \quad (25)$$

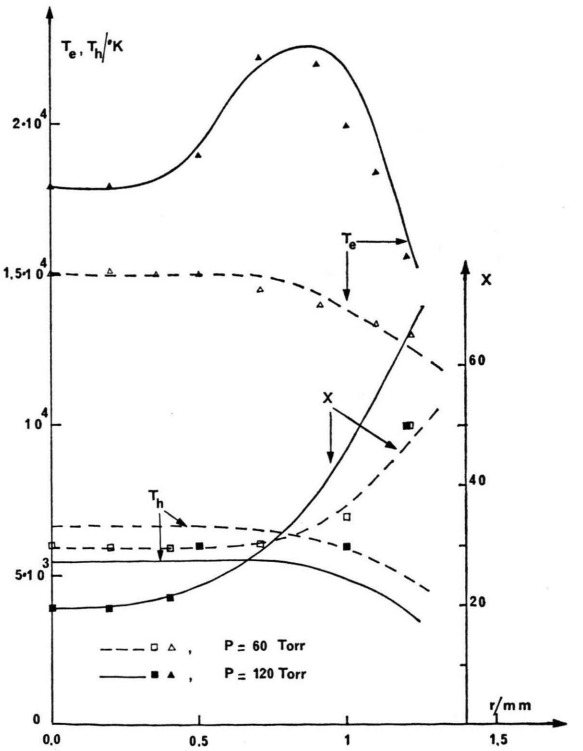


Fig. 10. Computed electron temperature ($T_e$), heavy particle temperature ($T_h$) and nonequilibrium parameter ($x = n_a/n_a^S$); triangles and squares are the solutions of the rate equations for the measured electron densities and atomic nitrogen excited state populations; curves are the solution of the electron energy equation.

Equations (24) and (25) are solved simultaneously with the rate equation for electron density [see Eqs. (18) and (19)],

$$\frac{1}{r}\frac{\mathrm{d}}{\mathrm{d}r}(r\,g_e) = k_r\,n_e{}^3(x-1) - \alpha\,n_e{}^2 \qquad (26)$$

for the experimental electron density distribution and with $T_e(r=0)$ and $x(r=0)$ obtained before as initial values. The solution yields now the heavy particle temperature $T_h(r)$. The corresponding results are shown by the curves in Fig. 10; they agree with those derived from the measured electronic state populations within the accuracy of measurements.

The important facts shown by these results are the following. The neutrals are overpopulated compared with the Saha equilibrium value ($x = n_a/n_a{}^S > 20$); the overpopulation decreases with increasing pressure (in the range studied). Discrepancies up to 60% are observed between the computed electron temperature and the highest excitation temperature (see Figure 6). The electron temperature, about three times higher than the heavy particle temperature, exibits an off-axis maximum like the Saha temperature does but it is also higher than the latter (about 10 to 15%). At the present, we cannot give an explanation of this effect. One reason could be that the Abel inversion in the boundary region of the plasma core gives inaccurate radial emission coefficients. We have especially checked this point and came to the conclusion that this cannot be the origin of this effect. It seems to be much more probable that the diffusion of $N_2$ and $N_2{}^+$ molecules, especially in metastable states, influences the atomic population in the boundary region. As has already been emphasized by Drawin, Fumelli and Weste [4] in their conclusion, electron temperatures deduced from an atomic non-LTE model may appear too high when the diffusion of molecular ions (and molecules) is not taken into account in the whole model. At the present, we try to refine the model in order to account for this influence.

## Conclusion

A nitrogen plasma jet operating in the pressure range $50 < P(\mathrm{Torr}) < 150$ shows a large departure from the equilibrium conditions essentially due to diffusion processes. The electron temperature and atom density are much higher than the equilibrium values. This conclusion agrees with the one of Shumaker [14] who made measurements on a nitrogen plasma under completely different experimental conditions. A two temperatures diffusion-dominated plasma yields a satisfactory interpretation of the experimental results. The model allows the computation of nonequilibrium parameter ($x = n_a/n_a{}^{\mathrm{Saha}}$), which is found to be higher than 20, and the heavy particle temperature which is found to be about twice to three times lower than the electron temperature.

*Acknowledgements*

Thanks are due to Professor H. W. Drawin for helpful discussions and valuable suggestions.

[1] D. R. Bates, A. E. Kingston, and R. W. P. McWhirter, Proc. Roy. Soc. London Ser. A **267**, 297 [1962].
[2] D. R. Bates, A. E. Kingston, and R. W. P. McWhirter, Proc. Roy. Soc. London Ser. A **270**, 155 [1962].
[3] D. R. Bates, Proc. Roy. Soc. London Ser. A **279**, 32 [1964].
[4] H. W. Drawin, M. Fumelli, and G. Weste, Z. Naturforsch. **20 a**, 184 [1955].
[5] H. W. Drawin, Z. Physik **186**, 99 [1965].
[6] C. Park, J.Q.S.R.T. **8**, 1633 [1968].
[7] C. H. Kruger, Phys. Fluids **13**, 1737 [1970].
[8] R. J. Giannaris and F. P. Iincropera, J.Q.S.R.T. **11**, 291 [1971].
[9] J. F. Uhlenbush and E. Fischer, Proc. IEE **59**, 578 [1971].
[10] C. Park, J. Plasma Phys. **9**, 187 [1973].
[11] H. W. Drawin and F. Emard, Z. Naturforsch. **28 a**, 1289 [1973].
[12] H. W. Drawin, F. Emard, and K. Katsonis, Z. Naturforsch. **28 a**, 1422 [1973].
[13] R. J. Giannaris and F. P. Incropera, J.Q.S.R.T. **13**, 167 [1973].
[14] J. B. Shumaker, J.Q.S.R.T. **14**, 19 [1974].
[15] A. Sy, Rev. Htes Temp. Réfract. **2**, 65 [1965].
[16] A. Catherinot and A. Sy, Special Report. PMI 73.1, Orléans University (unpublished).
[17] H. Griem, Plasma Spectroscopy, McGraw-Hill, New York 1964. a) Chap. 4; b) Chap. 4 and Tab. 4–5, p. 461; c) Chap. 5 and Tab. 5–8, p. 534.
[18] R. A. Hill, J.Q.S.R.T. **7**, 401 [1967].
[19] H. W. Drawin, Z. Physik **228**, 99 [1969].
[20] C. H. Kruger and M. Mitchner, Phys. Fluids **9**, 1953 [1967].
[21] C. H. Kruger, M. Mitchner, and V. Daybelge, A.I.A.A.J. **6**, 1712 [1968].
[22] S. Chapmann and T. G. Cowling, The Mathematical Theory of non-uniform Gases, Cambridge Univ. Press 1958.
[23] J. O. Hirschfelder, C. F. Curtiss, and R. B. Bird, Molecular Theory of Gases and Liquids, J. Wiley, New York 1964.
[24] R. M. Chmieleski and J. H. Ferziger, Phys. Fluids **10**, 2, 364 [1967].
[25] H. W. Drawin, Article in: Reactions under Plasma Condition, Chap. 3 and 4, Vol. I, ed. Venugopalan, J. Wiley, New York 1971.

[26] W. L. Wiese, H. W. Smith, and B. N. Glennon, Atomic Transition Probabilities, Vol. I, NSRDS-NBS 4 [1966].
[27] W. Lotz, Z. Physik **206,** 205 [1967].
[28] H. W. Drawin, Collision and Transport Cross Sections, report EUR-CEA-FC 383 (1966, revised 1967).
[29] C. Park, J.Q.S.R.T. **11,** 7 [1971].
[30] K. Smith, R. J. W. Henry, and P. G. Burke, Phys. Rev. **157,** 51 [1967].
[31] W. J. Karzas and R. Latter, Astrophys. J. Sup. Ser. **6,** 167 [1961].
[32] C. Peach, Mem. Roy. Astron. Soc. London **73,** 1 [1970].
[33] D. R. Bates and I. Estermann, Advance in Atomic and Molecular Physics, Vol. 2, 235, Academic Press, London 1966.
[34] J. A. R. Samson and R. B. Cairns, J. Opt. Soc. Am. **54,** 842 [1965].
[35] A. Catherinot, Thesis (1974) University of Orléans (France).
[36] C. Park, A.I.A.A.J. **7,** 1653 [1969].
[37] R. S. Devoto, Phys. Fluids **9,** 1230 [1966].
[38] R. S. Devoto, Phys. Fluids **10,** 2105 [1967].
[39] R. S. Devoto and C. P. Li, J. Plasma Physics **2,** 17 [1968].